A review of some recent developments in polarization-sensitive optical imaging techniques for the study of articular cartilage.

Stephen J Matcher
Department of Engineering Materials, University of Sheffield, Mappin Street, Sheffield S1 3JD, UK.
Telephone +44 114 22 25994
Fax +44 114 22 25943
S.J.Matcher@sheffield.ac.uk

Keywords: optical coherence tomography; polarization-sensitive optical coherence tomography; second harmonic generation, articular cartilage degeneration, osteoarthritis.

ABSTRACT

This article reviews recent developments in the optical imaging of articular cartilage using polarized-light methods, with an emphasis on tools that could be of use in tissue engineering approaches to treatment. Both second harmonic generation microscopy and polarization-sensitive optical coherence tomography are described and their potential role in the treatment of cartilage disorders such as osteoarthritis is suggested. Key results are reviewed and future developments discussed.

Introduction

Many painful and debilitating medical conditions manifest themselves most directly through abnormal properties of the extracellular matrix. This structure, which is composed chiefly of the body's most abundant structural protein – collagen - acts as the scaffold within which cells are maintained. A prime example of such a condition is osteoarthritis, which involves a gradual loss of the normal structure of hyaline cartilage and its replacement with fibrocartilage. Cartilage is an avascular tissue in which the cellular compartment, composed of chondrocytes, is completely reliant on the transport of nutrients via diffusion either from vascularised bone or from synovial fluid. Consequently therapeutic strategies are more limited than in most other tissues and currently all involve orthopaedic surgery. One of the most promising treatments is autologous chondrocyte implantation (ACI), which involves harvesting healthy cartilage from elsewhere on the joint, extracting the chondrocytes, amplifying them in culture and then re-implanting them into the site of the osteoarthritic lesion[1].

The need to remove healthy cartilage from the patient is clearly undesirable and has prompted interest in an entirely tissue-engineered solution to the problem. Tissue engineering is a rapidly emerging technique with potential to dramatically reduce the need for harvested autologous tissue in the management of severe burns[2] and its use to generate artificial articular cartilage is also generating intense interest. One particularly attractive approach is to harvest mesenchymal stem cells (MSC's) from the patient's bone marrow and culture these *ex-vivo*. It is known that by modifying the culture conditions of MSC's, they can be made to differentiate into a variety of phenotypes, including ones closely akin to native chondrocytes[3]. These differentiated MSC's can then be seeded into a 3-D scaffold made from natural or man-

made materials such as collagen, fibrin hydrogels, PLGA/PLLA copolymers[4], chitosan[5], silk[6] and others.

Optical techniques, especially minimally invasive imaging, have found a steady increase in application over the last 20 years. In ophthalmology for example, optical coherence tomography has emerged as the method of choice for non-invasive assessment of the retina and both OCT and confocal microscopy are under intense evaluation as methods of screening for epithelial cancers. However, optical techniques have not as yet made a major impact in orthopaedic care. In part this is explained by the limited depth-penetration into tissue (generally less than 1 mm) and the consequent difficulty of gaining access to structures such as bone, cartilage and synovium non-invasively. Although diffuse optical techniques have better depth penetration, they generally have poor spatial resolution. These methods have been suggested as a way of detecting abnormal blood oxygenation in the synovial membrane of rheumatoid articular joints however[7] and very recently photoacoustic tomography has been proposed to achieve a similar aim in small-animal models[8]. However these techniques are primarily looking for early-stage inflammatory changes in the joint, via changes in blood content.

In this article we will discuss optical assessment of cartilage changes using endogenous contrast mechanisms related to collagen microstructure. A number of clinical roles exist for such an assessment. Firstly, as we have noted, optical techniques have a potential role in the on-line monitoring of tissue-engineered constructs. Secondly, non-invasive or minimally invasive techniques may be of use for both detecting early-stage degenerative changes and for monitoring the response of cartilage to therapy. The limited tissue penetration of wholly optical techniques means that such assessments can only be carried out during interventions

that require the joint space to be opened. However this could encompass not only situations where osteoarthritis is already sufficiently advanced as to produce pain but also situations in which injury is sustained to related joint structures such as the anterior cruciate ligament without immediate collateral damage to the cartilage being directly evident. This latter situation could represent a new diagnostic opportunity as the prevention of osteoarthritic degeneration following such soft tissue injuries is a major goal of current orthopaedic practice. Techniques that augment the capabilities of conventional arthroscopy (especially by yielding sub-surface imaging) have a number of potential roles to play. Polarized light methods have high specificity to collagen microstructure and hence there is interest in their ability to detect pathological change in the deep cartilage zones before surface disruption becomes apparent. Clearly this would extend the therapeutic window for interventions; this is of considerable clinical interest given recent evidence that early intervention can potentially reverse pathological change[9]. Also it should be noted that the development and evaluation of new drugs does still require an animal model in most cases. The ability of optical techniques to provide longitudinal measurements in the same animal (currently animals must be sacrificed to yield specific time-points) could improve accuracy as well as reduce the cost of experiments.

Cartilage structure.

Articular cartilage is a complex structure, designed to withstand both compressive and shear forces due to articulation of the joint surfaces. It consists of a complex 3-D collagen/proteoglycan network within which water is trapped. The precise 3-D structure of the collagen has been the subject of study over the past century. **Figure 1** shows the classic "arcade" model of Benninghoff, in which collagen fibers arise in the subchondral bone, curve over as they reach the surface and then descend back to the subchondral bone[10]. At the

cartilage surface the fibers run parallel to the articular surface, forming the so-called "tangential" layer, of typical thickness 100 microns. Over the past two decades, high-resolution SEM imaging and cryofracture techniques have suggested that this model be revised. The work of Clark[11] and Jeffrey et al [12] suggest a model shown schematically in Figure 2, in which fibers arising from the subchondral bone form well-defined sheets or lamellae which curve over in the "transitional" layer to then lie parallel to the surface in the most superficial tangential layer. In this model the fibers do not descend back to the bone but terminate in the tangential layer. There is evidence from TEM and polarised light microscopy to further suggest that the fiber direction in alternate lamellae in the tangential layer is not uniform, but can vary by as much as 45 degrees between lamellae[13].

Within the collagen matrix, the interaction between water and proteoglycans generates a swelling pressure that helps provide the cushioning effect of cartilage. Osteoarthritis is associated with a gradual loss of proteoglycans and hyaluronic acid - with a subsequent reduction of the tissue's ability to generate a swelling pressure - and a replacement of hyaline cartilage with fibrocartilage. Once a fibrous lesion has begun to form it is essentially non-healing until a therapeutic intervention is performed. This might be an ACI procedure or the insertion of a tissue engineered construct. One of the goals of this article is to suggest ways in which optical techniques might contribute to these treatments.

Polarization-sensitive OCT of articular cartilage.

A number of labs are investigating the use of polarization-sensitive optical coherence tomography (PS-OCT) to study articular cartilage. PS-OCT has been used extensively to image birefringent tissues such as tendon[14], skin & muscle[15] and intervertebral disk[16]. Articular cartilage was also an early subject of investigation using both structural OCT[17] and

polarization-sensitive OCT[18]. Several excellent reviews of the PS-OCT technique exist e.g. de Boer and Milner[19]. OCT is an optical analogue of ultrasound imaging and is widely used to produce depth-resolved images of the retina[20]. Its primary mode of contrast is via refractive index differences between tissue layers. The essential difference between conventional and PS-OCT is that the former is sensitive only to the back-scattered light intensity versus depth, whereas the latter is sensitive to the polarization-state of the back-scattered light and thus, indirectly, to the presence of materials with a strong optical anisotropy such as collagen type-I and type-II. In this section we will briefly reacquaint ourselves with the optical parameters used to quantify OCT image contrast and optical anisotropy and describe the extent to which these can be quantitatively determined using various types of PS-OCT system. Where appropriate, commonly used mathematical symbols are introduced to denote these.

Tissue reflectivity R: This quantity is conventionally understood to indicate the total amount of optical power that is back-scattered from the sample at a fixed position (x,z). Then $R(x,z)$ is the most familiar OCT image, sometimes called a "structural" OCT image, which shows contrast wherever there is a boundary between different tissue types.

Linear birefringence (Δn): This property of an optical medium causes light beams linearly polarized in orthogonal directions to propagate at slightly different speeds i.e. the medium refractive index is slightly different for these two polarization states. The polarization direction with the higher refractive index is termed the "slow-axis" and the axis orthogonal to this and to the light propagation direction is the "fast-axis". For a positive uniaxial birefringent material such as collagen, this direction is co-incident with the axis of cylindrical symmetry of the collagen fiber provided the fiber lies in a plane orthogonal to the propagation direction of the light beam. In cases where this is not true a more complicated relationship exists, which is described in a later section. The difference in refractive index between the

slow and fast axes is termed the linear birefringence Δn. For most biological tissues its value typically ranges from 0 to 5×10^{-3}.

Phase retardation (δ): A consequence of linear birefringence is thus that after propagating a distance z, a phase difference is introduced between the oscillations in electric field resolved along these two directions. For a positive uniaxial material, the oscillation resolved along the fiber long-axis accumulates a phase-lead over that in the orthogonal direction. This is the most fundamental quantity that can be inferred from a PS-OCT measurement and is termed the phase-retardation δ. The magnitude of δ, in radians of phase, is given by the formula:

$$d = \frac{2p}{l}\Delta n\, z$$

Equation 1

Hence the birefringence Δn is derived by knowing the vacuum wavelength of the light λ and measuring δ at a known depth z in the tissue. A particularly simple way of doing this is to produce a so-called phase-retardation image i.e. instead of plotting tissue reflectivity R versus position i.e. $R(x,z)$, one plots $\delta(x,z)$. If the tissue has a spatially uniform Δn (tendon is a good example of such a material because it is structurally uniform at the resolution scale of OCT) then whereas $R(x,z)$ appears featureless, $\delta(x,z)$ has a "banded" appearance because whilst δ increases uniformly with increasing depth, being a phase angle in fact its value is only determined modulo 2π. Indeed, Equation 1 gives the "single-pass" phase retardation imparted on the light beam upon reaching the depth z; in OCT this beam is then reflected and propagates back through the overlying tissue before being detected, which doubles the actual phase retardation measured. Conventionally PS-OCT phase-retardation images display the single-pass retardation, which for a medium of uniform Δn thus display a banded structure which repeats over a distance z_{band} given by $z_{band} = 0.5\lambda/\Delta n$. Hence a simple way of measuring Δn is to measure the band-spacing in the retardation images.

Circular birefringence: For completeness we should mention that some optically anisotropic materials display circular rather than linear birefringence. Also known as “optical activity”, the phenomenon is associated with the presence of strongly chiral molecules (dextran is a potent biological source). The optical effect can be thought of as representing a difference in light propagation speed for right and left circularly polarised polarization states. Since a linearly polarized state can be decomposed into two circular polarized states of the opposite handedness, a simple consequence of optical activity is the rotation of the plane of polarization of a linearly polarized light beam. However because in OCT the beam propagates first down into the tissue and then after reflection at an interface propagates back up out of the tissue, circular birefringence cancels in double-pass and thus does not manifest itself in PS-OCT images.

Intrinsic and form birefringence: Δn yields information on the degree of optical anisotropy present in the sample however this anisotropy can arise at different length scales. Intrinsic linear birefringence arises due to anisotropy at the atomic or molecular scale and fundamentally is determined by the anisotropic distribution of electrical charge. This type of birefringence is an intrinsic property of the material and cannot be altered unless gross changes to the molecular structure are induced. Crystalline materials such as calcite are examples of intrinsically birefringent substances. However birefringence can be produced by another mechanism. If a materials consists of a background substance, into which is embedded a regular array of inclusions, then even if both the background material and the inclusions are optically isotropic and thus possess no intrinsic birefringence, if the refractive indices of these materials differ then the composite system can display birefringence, which is known as form birefringence[21]. The spatial length scale of the structure producing form birefringence is generally much larger than the molecular scale at which intrinsic birefringence is produced, but is still typically smaller than the wavelength of light. A crucial

distinguishing feature of form birefringence is that its value can be changed by changing the refractive index mismatch between the background material and the inclusions. Relating the quantitative value of birefringence to underlying physical properties is clearly more complicated in this case. Studies on Type-I collagen in tendon over the course of several decades has led to the consensus that this collagen type displays intense intrinsic positive birefringence due to the quasi-crystalline arrangement of the amino-acid residues that comprise the polypeptide chains of the collagen molecule alpha-chains[22]. This intrinsic birefringence can be further enhanced by binding acidic dyes such as picrosirius red to the collagen molecule. Weaker form birefringence is also observed but intrinsic birefringence is thought to dominate. Type-II collagen in articular cartilage has not been investigated to the same extent, but there is no strong reason to expect a significant difference.

Apparent and true birefringence: This terminology was introduced into the PS-OCT literature by the author's group in relation to our PS-OCT studies of articular cartilage[23]. The distinction is discussed more fully in the next section, but basically amounts to the observation that, regardless of its underlying origin – intrinsic or form – the birefringence value Δn that is extracted from a phase-retardation map is dependent not only on the underlying birefringence properties of the sample but also on the geometrical arrangement between the probing light beam and the 3-D spatial orientation of the fiber long-axis of the collagen. This effect is well-known in the field of crystal optics and is a classic optical lab demonstration that can be performed with a calcite crystal. When viewed at most angles, the anisotropic atomic arrangement of the calcium, carbon and oxygen atoms within the calcite crystal lattice gives rise to the phenomenon of "double-refraction", yielding a double-image of objects viewed through the crystal. However, along a unique axis in the crystal known as the "optic-axis" the arrangement of the atoms displays a 3-fold rotational symmetry which abolishes the apparent birefringence and hence the double-refraction phenomenon[24] because

birefringence requires a lack of rotational symmetry to be present. For a structure such as tendon, when viewed orthogonal to its long-axis the collagen fibers are aligned in such a way as to produce strong rotational asymmetry and so light experiences a very high birefringence. However, when viewed along the long-axis the fibers appear to form a semi-random array of packed cylinders seen end-on: this structure displays a high degree of rotational symmetry and hence the birefringence is weak. Thus the tissue sample displays very different "apparent birefringence" depending on how it is viewed even though the underlying optical properties are not changed. This phenomenon is very important in cartilage because the 3-D orientation of the fibers relative to the incident light beam can be highly variable.

Dichroism/diattenuation/biattenuance: In addition to displaying a different refractive index for orthogonal linearly polarised light beams, many optically anisotropic media can display different light absorption properties also. Polaroid® is the classic example, in which directionally aligned long-chain polymers of polyvinyl alcohol are conjugated to iodine to produce a medium that strongly absorbs light linearly polarized along the long-chain axis but absorbs orthogonally polarized light more weakly. Recently Kemp et al introduced the term "biattenuance" to describe broadly the same phenomenon, but extending the physical interpretation to include the effects of polarization-dependent back-scattering efficiencies by anisotropic embedded particles[25]. In principle it has been demonstrated that PS-OCT has the ability to measure the dichroism/diattenuation of biological samples in addition to the birefringence[26]. In practice the diattenuation effect seems to be significantly weaker than the birefringence effect and is frequently ignored in PS-OCT applications.

PS-OCT approaches.

Many designs for polarization-sensitive OCT scanners, i.e. systems that combine OCT imaging with polarimetry, have been proposed which vary in the degree of sophistication with

which they quantify the optical anisotropy of the medium. This is a potential source of confusion, because the effect of birefringence on the OCT image depends on the type of system one is using. No standard terminology for different PS-OCT systems has yet arisen, but for the purposes of this article we will define two generic classes of device.

Polarized-light OCT imaging systems. An early and simple method is to adapt a conventional OCT system to illuminate the specimen with linearly polarised light, the plane of polarization of which can be manually rotated relative to the sample [18,27]. This is sometimes called "single-detector" PS-OCT, although this term can be confusing because a number of designs for full "polarimetric" OCT systems that completely characterise the Jones matrix of the tissue sample have been proposed that also only requires a single light detector[28]. Polarized-light OCT systems have the benefit of simplicity but can also present difficulties in data interpretation because the degree of birefringence is generally not quantified, rather a qualitative judgement is made about the presence of "polarization-sensitivity" depending on whether the OCT image brightness or banding pattern appears to change when the plane of polarization of the incident light is altered. It is also important to note that the reflectivity image appears quite different to that of the true "polarimetric" OCT systems described next by virtue of the presence of a banding pattern; the position of the peaks and troughs of this pattern shift as the plane of polarization is altered but their spacing remains constant. This pattern arises because this simple approach to PS-OCT implicitly mixes the reflectivity and phase-retardation information

Polarimetric OCT imaging systems. These systems explicitly separate the image contrast parameters $R(x,z)$ and $\delta(x,z)$ and possibly also determine the local fast-axis orientation. For a structurally uniform tissue such as tendon, no banding is evident on the structural reflectivity image $R(x,z)$ however intense banding is observed on the phase retardation image $\delta(x,z)$. The

simplest such system uses a circularly polarized input light beam[29], which has the disadvantage however that it cannot easily be combined with fiber-optics because birefringence in the fiber itself will distort the circularly polarized light beam thus illuminating the sample with an arbitrary elliptical polarization state and thus invalidating the data analysis algorithms. However when used in a bulk-optics system the approach is a simple of way of determining $R(x,z)$ and $\delta(x,z)$ and also the local fast axis orientation[30]. More sophisticated schemes, in which more than one incident polarization state is used, have also been implemented[31,32,33]. Such schemes have the attraction that the effect of fiber optic birefringence can be compensated, which means that an endoscopic system can be envisaged that could be used during arthroscopy. There is at least one commercially available polarimetric OCT microscope on sale at the time of writing[34].

PS-OCT applications to in-vivo cartilage imaging.

Han et al have investigated the mechanisms of implanted chondrocyte integration into healthy tissue in a rabbit model using structural OCT[35] and Pan et al also noted the birefringent properties of normal porcine hyaline cartilage tissue using a polarized-light OCT system[27]. Chu et al have performed cadaveric and in-vivo human studies using a similar system and demonstrated that the absence of birefringence correlates with a reduced capacity for proteoglycan synthesis in response to IGF-1 stimulation[36]. Interestingly, this early degenerative change was demonstrated by PS-OCT at a potentially reversible stage.

3-D collagen structure determination using PS-OCT.

Much of the discussion concerning the use of PS-OCT to image cartilage centers on the measurement of the intrinsic birefringence and conclusions are often drawn about the

microscopic ordering of collagen fibers within the tissue based on the presence or absence of measurable intrinsic birefringence. Our work on equine cartilage however has emphasised that PS-OCT measures what we term the "apparent birefringence" which is determined not only by the biochemical constitution of the tissue but also by the 3-D structural arrangement of the fibres[23], an observation that has subsequently been confirmed by Xie et al[37], who went on to compare the 3-D structure of cartilage and meniscus using an approach similar to ours. Crudely modelling the birefringence properties of hyaline cartilage as being those of a uniaxial birefringent crystal then one sees intuitively that the apparent birefringence vanishes in cases where the dominant fibre orientation lies parallel to the beam propagation direction and reaches a maximum when these directions are mutually orthogonal. This can be formally described by the equation:

$$\frac{1}{n^2} = \frac{\sin^2 q_c}{n_e^2} + \frac{\cos^2 q_c}{n_o^2}$$

Equation 2

where the apparent birefringence (i.e. that directly measured by PS-OCT) is given by $\Delta n = n - n_o$, whereas the more fundamental underlying property is the "true birefringence" $n_e - n_o$. θ_c denotes the angle between the light propagation direction and the fibre long-axis. We have further demonstrated how it is possible to reconstruct both the 3-D orientation of fibres and the true birefringence by combining measurements of apparent birefringence made at a number of different illumination directions. Figure 3 (reproduced from[38] with permission) shows how the characteristic "banded" PS-OCT retardation image changes as one alters the incident beam illumination direction. With the beam perpendicular to the surface, no bands are evident, indicating a low value for Δn. In the absence of further information, this could indicate that $n_e - n_o$ is low but, by Equation 2, it could be that $n_e - n_o$ is large but $\theta_c \approx 0$. However images taken with an illumination direction that is inclined to the vertical (middle

and bottom rows) now show a banded appearance indicative of a higher value for Δn. This is now only consistent with near-vertically oriented fibres and further, the asymmetry of the images taken with equal but opposite beam inclination angles suggests that the fibres are not perfectly vertical but are tilted somewhat. These observations motivated us to develop what we have termed "variable-incidence-angle PS-OCT", in which multiple estimates of Δn taken with multiple illumination directions are least-squares fitted using Equation 2 to estimate the orientation angles of the fibres (polar angles θ and ϕ) and $n_e - n_o$. **Figure 4** (reproduced from[38] with permission) shows the results of this analysis applied to a quasi 2-D problem (i.e. using illumination directions confined to one plane and assuming that the fibres lie in this same plane) whereas **Figure 5** (reproduced from[39], with permission) shows a true 3-D determination obtained by using illumination directions in two orthogonal planes. Note especially how the 3-D orientation of the fibres changes from anterior to posterior orientation as one moves along the "sagittal ridge" in a medial to lateral direction and also how the fibres apparently change in azimuthal orientation from being parallel to the ridge in the posterior to inclined in the anterior.

On-line monitoring of tissue-engineered cartilage constructs.

Cartilage constructs are currently being developed using a variety of approaches, but in general all involve constructing some form of acellular scaffold into which cells are seeded. It is hoped that the cells are then able to actively generate new matrix proteins such as collagen and that ultimately this regenerated collagen can assume the role of the native ECM that has been lost due to degeneration. An interesting question then arises relating to the scaffold architecture of the construct. Many scaffold production techniques produce randomly-aligned fibres (e.g. electrospinning), others are capable of generating directionally aligned fibres, which could in turn promote directionally aligned collagen production[40]. Recently, for

example, Moutos et al demonstrated cartilage scaffolds created using a 3-D microscale weaving technique that is capable of producing scaffolds with anisotropic mechanical properties[41.] In addition, there is evidence that external stimuli such as mechanical loading can promote aligned collagen fibres in tissues such as tendon and mathematical models have been developed to predict the causal relationship between applied stress and collagen alignment in cartilage[42]. So the possibility exists to try to create a synthetic cartilage construct whose collagen alignment matches that of the native tissue at the site of implantation. To achieve this end we clearly need a technique that can quantify the 3-D collagen structure of both native and tissue engineered cartilage. It would be beneficial to know roughly how the collagen fibres are oriented at various sites in normal cartilage so that an 'atlas' can be created. This 3-D orientation distribution is likely to reflect the 3-D stress distribution that the cartilage experiences in normal circumstances. Then a technique that could monitor the production of collagen in a bioreactor would allow the continuous monitoring of how well the tissue construct ECM matches that of the host tissue, during the development of the construct. Many techniques exist that can determine collagen fibre organisation in tissues, including SAXS[43], diffusion-tensor MRI[44] and FT-IR polarimetry[45] but none are well adapted to the needs of on-line monitoring. In this application, an ideal method should possess the following characteristics:

A. Provide full 3-D information on the orientation of the collagen fibres to a depth of up to 1 mm in biological tissue, non-destructively and with a depth-resolution of around 5-10 microns.

B. Rapid imaging speeds (fractions of a second per 2-D scan).

C. Use non-ionising radiation, making it potentially applicable in vivo.

D. Have the potential to be applied endoscopically e.g. during arthroscopic examination of articular cartilage.

From the previous discussions we suggest that PS-OCT, especially if extended to true 3-D fiber orientation determination using the variable-incidence-angle approach, may be ideally suited to fulfilling this need.

Real-time cartilage histology using non-linear microscopy.

During a procedure such as ACI, the orthopaedic surgeon must remove diseased cartilage from the site of the lesion. In order to gauge the extent of tissue to remove, the surgeon relies on visual assessment of the cartilage surface, however this assessment is of necessity subjective. It would be potentially of benefit if the surgeon could have a real-time quantitative assessment of the integrity of the cartilage extracellular matrix (ECM) of the tissue removed, so that the degree of resection is minimized.

Conventionally, tissue viability is assessed by histology however this process is laborious and operator-dependent as it generally requires chemical staining of the samples before observing them under a light-microscope. To make real-time histology viable requires a microscopy technique that uses endogenous rather than exogenous contrast. Preferably it would also be sensitive to cell morphology and extracellular matrix structure and yield information deep into the tissue without requiring complicated and time-consuming mechanical sectioning.

A tool well suited to meet these requirements is non-linear microscopy, especially and second-harmonic generation microscopy. Second-harmonic generation is a non-linear optical phenomenon that has been observed in collagen-rich tissues for several decades[46]. The basis of the technique is the observation that, at sufficiently high light intensities, the dielectric susceptibility becomes a non-linear function of the applied field, so that the bulk polarizability becomes expressible as (with the summation convention implied):

$$P_i = e_0\left(c_{ij}^{(1)}E_j + c_{ijk}^{(2)}E_jE_k + c_{ijkl}^{(3)}E_jE_kE_l + \mathbf{K}\right)$$

Equation 3

When the second order susceptibility tensor $\chi^{(2)}$ becomes significant, an applied field oscillating sinusoidally at angular frequency ω gives rise to an emitted field with angular frequency 2ω.

Interestingly the phenomenon is sensitive not just to the abundance (i.e. volume fraction) of collagen fibrils within the optical focus but also on their degree of sub-microscopic spatial ordering. This is because SHG is a coherent optical phenomenon that requires an absence of mirror-inversion symmetry in order to occur and hence is maximally efficient when the focal volume contains asymmetric molecular oscillators that are aligned in the same direction in space. In addition, the polarization state of the emitted SHG radiation gives direct information on the dominant alignment of collagen fibres on sub-micron scales. Freund et al have shown that for biological tissues showing a strong uniaxial structure (i.e. C_∞ symmetry) excited by radiation with energy well below that of resonant electronic transitions (so that Kleinmann symmetry can be assumed) then the expression for the polarization state of emitted SHG radiation simplifies considerably. For fibres lying in the x-z plane and uniaxially oriented in the z-direction, illuminated by a laser beam propagating in the y-direction whose field is $\mathbf{E}^{(1)}$, the induced second-order polarizability $\mathbf{P}^{(2)}$ simplifies to:-

$$\begin{aligned} P_z^{(2)} &= r\left[E_z^{(1)}\right]^2 + \left[E_x^{(1)}\right]^2, \\ P_x^{(2)} &= 2E_x^{(1)} \cdot E_z^{(1)} \end{aligned}$$

Equation 4

where $r\left(= c_{zzz}^{(2)} / c_{zxx}^{(2)}\right)$, by virtue of the symmetries assumed, completely defines the full second-order susceptibility tensor and typically takes on the value of 1.8 for rat-tail tendon[46]. As the emitted intensity is proportional to the squared-modulus of the polarizability, it follows

that if the sample is illuminated with linearly polarized light, with an angle α between the z-axis the plane-of-polarization, then the x and z components of the emitted SHG field are

$$I_z^{(2)}(a) \propto \left[r\cos^2 a + \sin^2 a \right]^2 \quad I_x^{(2)}(a) \propto \left[\sin 2a\right]^2,$$

Equation 5

and hence if the total emitted intensity $I_{tot}^{(2)}(a) = I_z^{(2)}(a) + I_x^{(2)}(a)$ is recorded versus α, then for $\rho \approx 2$ the signal will display a well-defined global minimum when α = 90° or 270°, which permits a determination of the orientation of the collagen fibres. Also, a crude determination of the value of ρ is possible, for example if $\rho \approx 0$ then the signal will display four minima of roughly equal amplitude per 360° instead of two.

Two-photon fluorescence is an inelastic optical scattering process which is fundamentally incoherent. It does not give direct information on collagen fibre orientation but adds a rich gamut of biochemical information. Two-photon autofluorescence has been shown to reveal elastin content[47] as well as locating cell nuclei and mitochondria and potentially yielding information on the redox potential of the cells[48]. Conveniently, both SHG and TPEF can be performed on the same microscope platform, requiring only a simple filter change to switch between the two modalities.

It should be stressed that neither SHG or TPEF microscopy are good candidates for *in-situ* monitoring of articular cartilage, because the mean optical powers needed are high and because the optical platform is intrinsically bulky and hard to combine with minimally invasive fiber optic technology. Also the requirement to maintain a high peak power in the focal spot means that practically it is hard to image deeper then a 100-200 microns even using long (several seconds per 2-D en-face image) integration times. However, as noted above, the

technique may find a niche in providing on-line histological assessment of the cellular morphology and collagen microstructure in the superficial layer of cartilage sections excised by a surgeon during procedures such as ACI. As a technique it is thus worthy of assessment and to this end it is important to understand the nature of the signals produced by both normal and diseased cartilage.

The first systematic study of articular cartilage using non-linear microscopy was performed by Yeh et al [49]. Using second-harmonic generation microscopy they showed that the extracellular matrix of normal bovine articular hyaline cartilage gives rise to significant amounts of second harmonic light but little two-photon fluorescence when excited with light of wavelength above 800 nm. However the signal from normal tissue did not appear to be strongly polarization-sensitive, suggesting that this tissue apparently lacks a unique fibre alignment direction. In contrast, the fibrocartilage deposited at sites of osteoarthritic change did produce a signal with a pronounced polarization-sensitivity.

Polarization-sensitivity of SHG signals from articular cartilage.

Both the morphology and the polarization-sensitivity of cartilage SHG has recently been studied in more detail in our own laboratory by Mansfield et al, using equine rather than bovine samples[50]. **Figure 6** shows images of SHG and fluorescence taken from various sites corresponding to normal (site a), osteoarthritic (site c) and "transitional" i.e. close to a visible lesion but not itself displaying disruption of the surface (site b). Note how the morphological appearance of both the matrix and the chondrocytes changes markedly in osteoarthritis. The matrix of fibrocartilage is noticeably more "rippled" than that of normal or transitional cartilage. Interestingly, note also how the "pericellular matrix" of the chondrocytes appears significantly brighter in the transitional cartilage than in the normal cartilage, whilst this

bright halo vanishes in the highly degenerated fibrocartilage. Using a half-wave plate to rotate the incident polarization direction and an unpolarized light detector, curves of $I_{tot}^{(2)}(a)$ can be produced at various sites on the equine third metacarpophalangeal joint, as functions of depth. **Figure 7** shows the results. (Note that for the purposes of clarity the profiles at different depths have been normalized to the same mean intensity and the 'Polarization angle' is actually $\approx \alpha+90°$, with some uncertainty due to the difficulty in establishing the absolute fibre orientation in superficial cartilage by independent means such as a 'split-line' experiment). A key observation is that even in visibly normal equine metacarpophalangeal cartilage (upper graph), there is a marked polarization sensitivity in the SHG signal, qualitatively similar to that obtained from rat-tail tendon. This is in contrast to Yeh et al's findings for bovine femoral/tibial/patellar cartilage. Furthermore, there is also a change in the angular pattern with depth, such that the usual double-peaked graph tends to a more complicated quadruple-peaked graph at greater depths, with the surface maxima being preserved whilst the surface minima become new maxima. Given that the number of global minima predicted by Equation 5 increases to four when ρ falls towards unity, one might be tempted to interpret this change as a depth-dependent structural variation in the effective value of ρ, possibly due to one moving from the superficial zone of well-ordered fibres into the deeper transitional region, where the fibre order is more random. However this explanation is undermined by the fact that Equation 5 predicts that the minima would remain in the same location whilst the maxima would become new minima, the opposite of what is observed. Another possible interpretation of this result is that accumulated tissue birefringence causes a change in the polarization-state of the light with increasing depth and thus distorts the pattern of SHG signal versus polarization angle. This effect has been modelled previously[51], although the precise effect on the polarization curve was not explicitly noted. A simple model for the effect of birefringence on the SHG curve can be derived if one ignores effects due to the large numerical aperture of the

focussed beam. Although clearly not realistic in the case of SHG microscopy, it is nevertheless helpful to gain a simple insight. Consider the geometry shown in **Figure 8**. Following the conventions used by Freund et al[46], we place the long-axis of the SHG-generating fibrillar structure along the *z*-axis and orient the incident electric field vector at an angle to the *z*-axis and in the *x*-*z* plane. To include birefringence we further assume that this incident field propagates through a birefringent plate whose slow axis (SA) makes an angle θ to the z-axis before irradiating the fibril. Note that *a-priori* one might expect θ to equal zero as the long-axis of collagen fibres corresponds to the optical slow axis[22]. However to keep the discussion general we will include the possibility that θ is not zero, which could potentially occur if SHG generation arises from structures of a smaller spatial scale than those producing linear birefringence. To calculate the SHG signal we will follow the procedure of Freund et al. In the absence of birefringence the steps are:

1. Resolve $\mathbf{E}^{(1)}$ along z and x-axes, yielding components $E^{(1)}_z = |\mathbf{E}^{(1)}| \cos \alpha$ and $E^{(1)}_x = |\mathbf{E}^{(1)}| \sin \alpha$ respectively.
2. Calculate the 2nd-order polarisations along *z* and *x* via the equations

$$P^{(2)}_z = \rho[E^{(1)}_z]^2 + [E^{(1)}_x]^2$$

$$P^{(2)}_x = 2E^{(1)}_x \bullet E^{(1)}_z$$

Equation 6

3. Calculate the unpolarised SHG intensity using $I_{SHG} \propto |P^{(2)}_x|^2 + |P^{(2)}_z|^2$

To account for birefringence, which introduces a relative phase retardation δ (radians) to the field component polarized along SA, we simply adapt step 1 of the above procedure by resolving the incident E-field parallel (||) and orthogonal (⊥) to SA, applying a phase factor $\exp(i\,\delta)$ to the $E_{\|}$ component, resolving the new E-field along *z* and *x* and then applying the above equations to calculate I_{SHG}. Hence:-

$$E_{\parallel}^{(1)} = E^{(1)} \cos g \cdot \exp(id)$$
$$E_{\perp}^{(1)} = E^{(1)} \sin g$$
$$E_{z}^{(1)} = E_{\parallel}^{(1)} \cos q + E_{\perp}^{(1)} \sin q = E^{(1)}(\cos q \cdot \cos g \cdot \exp(id) + \sin q \cdot \sin g)$$
$$E_{x}^{(1)} = E_{\parallel}^{(1)} \sin q - E_{\perp}^{(1)} \cos q = E^{(1)}(\sin q \cdot \cos g \cdot \exp(id) - \cos q \cdot \sin g)$$

For simplicity, taking $E^{(1)}$ to be 1.0…

$$E_{z}^{(1)} = \cos q \cdot \cos(q - a) \cdot \exp(id) + \sin q \cdot \sin(q - a)$$
$$= \cos a + \frac{(\exp(id) - 1)}{2}(\cos a + \cos(2q - a))$$

Likewise

$$E_{x}^{(1)} = \sin a + \frac{(\exp(id) - 1)}{2}(\sin a + \sin(2q - a))$$

Equation 7

The calculation of I_{SHG} then follows using steps 2 and 3 above. Note that δ can be complex, in which case the imaginary part represents the "diattenuance" of the tissue i.e. the differential absorption of light polarized along the direction SA relative to that of light polarized orthogonal to this direction[25]. We have used fluorescence polarimetry to quantify Im(δ) for both equine tendon and equine hyaline cartilage, finding apparent values of 2.65×10^{-4} for tendon but significantly less for cartilage[50]. We have previously estimated Re(δ) for equine tendon[38], obtaining a value of 4×10^{-3} and thus suggesting that realistic values for Im(δ)/Re(δ) for collagen-rich connective tissues might lie in the range 0 to 0.06. Figure 9 shows simulated versions of **Figure 7**, calculated using **Equation 6** and Equation 7, with the profiles at different depths normalized to the same mean intensity.

Both images are calculated using ρ = 1.8, θ = 0° and Im(δ)/Re(δ) = 0.2. The upper image is calculated with Re(δ) = 1.2×10^{-3} so that a quarter waveplate is accumulated by a depth of 170 microns whilst the lower has Re(δ) = 0.7×10^{-3}. Note the good qualitative agreement with

Figure 7 (sites 1 and 3), with the desired change from 2 to 4 minima and the transformation of the surface minima to maxima with increasing depth for the upper image and the maintenance of two minima over most of the depth in the lower image.

The implication of these data seems to be that both morphological and polarimetric information can be obtained using SHG microscopy on normal and diseased cartilage and that distinct differences exist between the normal and abnormal tissues. Polarimetric data suggests a fall in birefringence at sites of both advanced osteoarthritic change (i.e. a visibly disrupted surface) and earlier stages of degeneration, when no surface disruption is evident. Hence we suggest that non-linear microscopy is worthy of more detailed study as a potential tool for performing real-time histology of excised articular cartilage.

Discussion and conclusions.

Polarized light microscopy was one of the earliest physical techniques to be used to study the morphology of collagen-rich biological tissues. However its use in recent years has diminished as x-ray diffraction has become the workhorse of structural biology whereas clinical imaging demands tools that can be applied in-vivo to intact, unstained tissues. The use of optical polarimetry to study connective tissues is however undergoing a revival due to the introduction over the last 10 years of new imaging technologies.

The physical anisotropy of connective tissues such as articular cartilage give rise to strongly anisotropic optical properties such as linear birefringence and second-harmonic generation. With the advent of non-destructive “optical biopsy” tools such as PS-OCT and SHG microscopy, these optical signals have the potential to provide valuable diagnostic information that could aid the management of connective tissue disorders such as

osteoarthritis. In this article we have reviewed these two imaging platforms and have speculated on potential roles that they may play in the treatment of pathologies of the extracellular matrix such as osteoarthritis. We have focussed on treatments for osteoarthritis that involve the in-situ replacement of damaged cartilage, such as ACI or tissue engineering, and have highlighted ways that these optical tools might potentially benefit such treatments.

PS-OCT is a tool ideally suited to monitoring the development and integration of 3-D tissue engineered cartilage constructs both in the bioreactor and in-situ. We have noted here how the complicated 3-D structure of cartilage collagen requires the use of multiple illumination directions, otherwise the resulting apparent birefringence can grossly underestimate the true birefringence. By fully developing this method, one can envisage a rapid, non-destructive optical technique yielding depth-resolved information on the 3-D zonal structure of such constructs and allowing a real-time comparison of this with that of the native cartilage at the site of implantation. This could bring tissue engineering of cartilage to a new level of refinement.

SHG microscopy, and its close relative TPEF microscopy, has been shown to provide images that display clear morphological differences when comparing normal cartilage with visually damaged cartilage and also cartilage located in close proximity to the damaged area. Both the gross structure of the extracellular matrix and the appearance of the pericellular matrix surrounding the chondrocytes display differences, with a strongly fibrillated appearance of the extracellular matrix characterising the osteoarthritic lesion and enhanced pericellular image brightness apparently characterising earlier stage degeneration. As SHG microscopes become cheaper and more portable (e.g. through the development of low-cost mode-locked fibre

lasers), SHG microscopy may find a role in the real-time histological assessment of excised articular cartilage.

The whole field has potential for further development, as improved technology improves imaging speeds and reduces costs. Of equal importance, improved data analysis and more rigorous comparisons with gold-standard techniques will deepen our understanding of the origin and correct interpretation of the polarimetric signals.

ACKNOWLEDGMENTS.

This article summarises the work of many collaborators. I am indebted to the following people for helpful discussions and for contributing to the work described herein: Marco Bonesi, Aileen Crawford, Sergey Gangnus, Paul Hatton, James Jacobs, Karen Knapp, Jessica Mansfield, Igor Meglinski, Julian Moger, Roy Sambles, Nadya Ugryumova and Peter Winlove. Generous financial support from the Coote Fund, the Arthritis Research Campaign, the Engineering and Physical Sciences Research Council, the Medical Research Council and the Royal Society is also gratefully acknowledged.

Figure Captions

Figure 1 The orientation of collagen fibrils in normal articular cartilage, as expounded in the classic “arcade” model of Benninghoff. Collagen fibres arise from the subchondral bone where they are radially oriented, curve over to lie parallel to the cartilage surface in the superficial “tangential” layer then descend back to the underlying bone. The tangential layer is generally less than 100 microns thick, whilst the majority of the full thickness of the cartilage (1 mm or so) is occupied by the transitional and radial zones.

Figure 2. A contemporary view of collagen organisation in cartilage, based on cryofracture SEM imaging of cartilage in 3 mutually orthogonal planes, one of which is determined by the local “split-line” direction (reproduced from Jeffrey et al). The collagen fibres arise from the bone and curve over to form a lamellar network in the tangential zone, but do not descend back to the bone.

Figure 3. PS-OCT retardance images of equine cartilage as a function of the incident beam polar angle. The lack of banding in the upper image (corresponding to a vertical incident beam) suggests that the collagen fibres are oriented close to the vertical also, as confirmed by the appearance of stronger banding (i.e. birefringence) for angles of incidence away from the vertical (middle and lower curves). Reproduced from[38] with permission.

Figure 4. Fibre polar angles at various point around the sagittal ridge of the equine third metacarpophalangeal joint, as determined by applying **Equation 2** to birefringence values extacted from image sets similar to **Figure 3**. Reproduced from[38] with permission.

Figure 5. Schematic representation of 3-D structure of cartilage fibres in the equine third metacarpophalangeal joint as derived from multi-angled PS-OCT measurements. Reproduced from[38] with permission.

Figure 6. Illustrating the morphological appearance of normal (upper row), diseased (low row) and intermediate (middle row) of SHG (left column) and TPF (right column) images of equine cartilage. (Reproduced from[50] with permission).

Figure 7. Total SHG intensity versus polarization angle, for normal (upper row), diseased (lower row) and intermediate (middle row) samples of equine cartilage (Reproduced from[50]).

Figure 8. Schematic showing the relationship between a collagen fibril (oriented along the z-axis), the applied electric field $\mathbf{E}^{(1)}_{in}$ and the fast-axis (FA) of the birefringent material lying between the fibril and the incident laser beam. The incident electric field vector subtends an angle α to the fibrillar long axis. The birefringence slow-axis subtends an angle θ (for completeness, not necessarily equal to zero) to the z-axis.

Figure 9. Simulated versions of Figure 7 using Equation 6 and Equation 7 with parameters $\rho = 1.8$, $\theta = 0$, $\mathrm{Im}(\delta)/\mathrm{Re}(\delta) = 0.2$ and $\mathrm{Re}(\delta)$ equivalent to a quarter-wave plate at depth 170 microns (upper graph) and 275 microns (lower graph).

References.

1 Cole BJ, and M D'Amato "Autologous chondrocyte implantation", *Operative Techniques in Orthopaedics*, 11(2): pp 115-131 (2001).

2 MacNeil S, "Progress and opportunities for tissue-engineered skin", *Nature* 445(7130): 874-880 (2007).

3 Atkinson BL, Fantle KS, Benedict JJ, Huffer WE, GutierrezHartmann A, "Combination of osteoinductive bone proteins differentiates mesenchymal C3H/10T1/2 cells specifically to the cartilage lineage", JOURNAL OF CELLULAR BIOCHEMISTRY 65(3), 325-339 (1997).

4 Canceddaa R, Dozina B, Giannonia P, Quarto R, "Tissue engineering and cell therapy of cartilage and bone", *Matrix Biology* 22 81–91 (2003).

5 Lahiji A, Sohrabi A, Hungerford DS, Frondoza CG, "Chitosan supports the expression of extracellular matrix proteins in human osteoblasts and chondrocytes", JOURNAL OF BIOMEDICAL MATERIALS RESEARCH 51(4), 586-595 (2000).

6 Wang YZ, Blasioli DJ, Kim HJ, Kim HS, Kaplan DL , "Cartilage tissue engineering with silk scaffolds and human articular chondrocytes", BIOMATERIALS 27(25), 4434-4442 (2006).

7 Hielscher AH, Klose AD, Scheel AK, Moa-Anderson B, Backhaus M, Netz U, Beuthan J, "Sagittal laser optical tomography for imaging of rheumatoid finger joints", *Phys. Med. Biol.* 49(7): 1147-1163 (2004).

8 Wang XD, Chamberland DL, Carson PL, Fowlkes JB, Bude RO, Jamadar DA, Roessler BJ "Imaging of joints with laser-based photoacoustic tomography: An animal study", MEDICAL PHYSICS, 33(8): 2691-2697 (2006).

9 Studer RK and Chu CR, “p38 MAPK and COX2 inhibition modulate human chondrocyte response to TGF-beta,” *J. Orthop. Res.* 23(2), 454–461 (2005).

10 Benninghoff A, “Form und Bau der Gelenkknorpel in ihren Beziehungen zur Function. II. Der Aufbau des Gelenkknorpels in seinen Beziehungen zur Function. Zeitschrfit fur Zellforschung and mikroskopische”, *Anatomie* 2, 783-862 (1925).

11 Clark JM, “The organisation of collagen fibrils in the superficial zones of articular cartilage”, *J. Anat.* 171, pp. 117-130, (1990).

12 Jeffery AK, Blunn GW, Archer CW and Bentley G, “3-Dimensional Collagen Architecture In Bovine Articular-Cartilage”, JOURNAL OF BONE AND JOINT SURGERY-BRITISH VOLUME 73(5): 795-801 (1991).

13 Ortmann R, “Use of polarized light for quantitative determination of the adjustment of the tangential fibres in articular cartilage”. *Anatomy and Embryology* 148, 109-120 (1975).

14 de Boer JF, Milner TE, van Gemert, MJC and Nelson JS, “Two-dimensional birefringence imaging in biological tissue by polarization-sensitive optical coherence tomography”, Optics Letters 22(12): 934-936 (1997).

15 de Boer JF, Milner TE and Nelson JS, “Determination of the depth-resolved Stokes parameters of light backscattered from turbid media by use of polarization-sensitive optical coherence tomography”, *Optics Letters* **24(5)**: 300-302 (1999).

16 Matcher SJ, Winlove CP and Gangnus SV. “The collagen structure of bovine intervertebral disc studied using polarization sensitive optical coherence tomography”, *Phys. Med. Biol.* **49**: 1295 – 306 (2004).

17 Herrmann JM, Pitris C, Bouma BE, Boppart SA, Jesser CA, Stamper DL, Fujimoto JG and Brezinski ME, “High resolution imaging of normal and osteoarthritic cartilage with optical coherence tomography”, *The Journal of Rheumatology* **26**, 627-635 (1999).

18 Drexler W, Stamper D, Jesser C, Li XD, Pitris C, Saunders K, Martin S, Lodge MB, Fujimoto JG, Brezinski ME, “Correlation of collagen organization with polarization sensitive imaging of in vitro cartilage: Implications for osteoarthritis”, JOURNAL OF RHEUMATOLOGY 28(6):1311-1318 (2001).

19 de Boer JF, Milner TE, “Review of polarization sensitive optical coherence tomography and Stokes vector determination”, JOURNAL OF BIOMEDICAL OPTICS 7(3): 359-371 (2002).

20 Zysk AM, Nguyen FT, Oldenburg AL, Marks DL, Boppart SA “Optical coherence tomography: a review of clinical development from bench to bedside”, *J. Biomed. Opt.* 12(5), 051403 (2007).

21 Born and Wolf, “Principles of Optics” Chapter 14. Pergamon Press.

22 Wolman M and Kasten FH. “Polarized light microscopy in the study of the molecular structure of collagen and reticulin”. *Histochemistry*, 85:41–9 (1986).

23 Ugryumova N, Attenburrow DP, Winlove CP and Matcher SJ. “The collagen structure of equine articular cartilage, characterized using polarization-sensitive optical coherence tomography”, *Journal Physics D: Appl. Physics* 38: 2612–9 (2005).

24 Hecht E, “Optics” Chapter 8. Addison-Wesley.

25 Kemp NJ, Zaatari HN, Park J, Rylander HG, and Milner TE, “Form-biattenuance in fibrous tissues measured with polarization-sensitive optical coherence tomography (PS-OCT)”, *Opt. Express* **13**, 4611-4628 (2005).

26 Jiao SL and Wang LHV, “Jones-matrix imaging of biological tissues with quadruple-channel optical coherence tomography”, JOURNAL OF BIOMEDICAL OPTICS 7(3): 350-358 (2002).

27 Pan Y, Li Z, Xie T and Chu CR, “Hand-held arthroscopic optical coherence tomography for in vivo high-resolution imaging of articular cartilage”, *Journal of Biomedical Optics* 8(4): 648–654 (2003).

28 Jiao S, Todorovic´ M, Stoica G, and Wang LV, “Fiber-based polarization-sensitive Mueller matrix optical coherence tomography with continuous source polarization modulation”, *Applied Optics*, 44(26): 5463- 5467 (2005).

29 Hee MR, Huang D, Swanson EA and Fujimoto JG “Polarization-sensitive low-coherence reflectometer for birefringence characterization and ranging”, *JOSA* 9(6): 903-908 (1992).

30 Hitzenberger CK, Gotzinger E, Sticker M, Pircher M, Fercher AF, “Measurement and imaging of birefringence and optic axis orientation by phase resolved polarization sensitive optical coherence tomography”, *OPTICS EXPRESS* 9(13): 780-790 (2001).

31 Saxer CE, de Boer JF, Hyle Park B, Zhao Y, Chen Z and Nelson JS, “High-speed fiber-based polarization-sensitive optical coherence tomography of in vivo human skin.” *Opt. Lett.* 25(18): 1355-1357 (2000).

32 Zhang J, Guo S, Jung W, Nelson JS, Chen Z, “Determination of birefringence and absolute optic axis orientation using polarization-sensitive optical coherence tomography with PM fibers”, 11(24) *Opt Express* 3262-3270 (2003).

33 Davé DP, Akkin T, and Milner TE, “Polarization-maintaining fiber-based optical low-coherence “reflectometer for characterization and ranging of birefringence”, *Opt. Lett.* 28(19), 1775-1777 (2003).

34 Thorlabs Inc.

35 CW Han, CR Chu, N Adachi, A Usas, FH Fu, J Huard and Y Pan, “Analysis of rabbit articular cartilage repair after chondrocyte implantation using optical coherence tomography”, *Osteoarthritis and Cartilage* 11: 111–121, (2003).

36 Chu CR, Izzo NJ, Irrgang JJ, Ferretti M, Studer RK, “Clinical diagnosis of potentially treatable early articular cartilage degeneration using optical coherence tomography”, *Journal of Biomedical Optics* 12(5), 051703 (2007).

37 Xie TQ, Guo SG, Zhang J, Chen ZP, Peavy GM “Use of polarization-sensitive optical coherence tomography to determine the directional polarization sensitivity of articular cartilage and meniscus”, *J. Biomed. Opt.* 11:6, 05385RR (2006).

38 Ugryumova N, Gangnus SV and Matcher SJ. “Three-dimensional optic axis determination using variable-incidence-angle polarization optical coherence tomography”. *Optics Letters*; 31: 2305-7 (2006).

39 Ugryumova N, Bonesi M and Matcher SJ, “Determination of 3D optic axis orientation in cartilage by Polarization-Sensitive Optical Coherence Tomography”, *Proc. SPIE* 6858, 68580I (2008)

40 Zehbe R, Gross U, Schubert H , “Oriented collagen-based/hydroxyapatite matrices for articular cartilage replacement”, *Bioceramics 16: Key Engineering Materials*, 254-2: 1083-1086 (2004).

41 Moutos FT, Freed LE and Guilak F, “A biomimetic three-dimensional woven composite scaffold for functional tissue engineering of cartilage”, *Nature Materials* 6: 162-167 (2007).

42 Wilson W, Driessen NJB, van Donkelaar CC, Ito K, “Prediction of collagen orientation in articular cartilage by a collagen remodeling algorithm”, *Osteoarthritis Cartilage* 14 (11): 1196-1202 (2006).

43 Moger CJ , Barrett R , Bleuet P , Bradley DA , Ellis RE , Green EM et al. Regional variations of collagen orientation in normal and diseased articular cartilage and subchondral bone determined using small angle X-ray scattering (SAXS). *Osteoarthritis Cartilage*; 15: 682-7 (2007).

44 Denga X, Farley M, Nieminena MT, Gray M, Burstein D, "Diffusion tensor imaging of native and degenerated human articular cartilage", *Magnetic Resonance Imaging* 25: 168–171, (2007).

45 Bi X, Li G, Doty SB and Camacho NP, "A novel method for determination of collagen orientation in cartilage by Fourier transform infrared imaging spectroscopy (FT-IRIS)", *Osteoarthritis Cartilage* **13**,1050-8 (2005).

46 Freund I, Deutsch M, and Sprecher A, "Connective-Tissue Polarity - Optical 2nd-Harmonic Microscopy, Crossed-Beam Summation, and Small-Angle Scattering in Rat-Tail Tendon", *Biophys. J.* 50, 693-712 (1986).

47 So PTC, Kim H and Kochevar IE , "Two-photon deep tissue ex vivo imaging of mouse dermal and subcutaneous structures" *Opt. Express* 3(9), 339-350 (1998).

48 Huang S, Heikal AA, and Webb WW, "Two-Photon Fluorescence Spectroscopy and Microscopy of NAD(P)H and Flavoprotein", *Biophys. J.* 82, 2811–2825 (2002).

49 Yeh AT, Hammer-Wilson MJ, Van Sickle DC, Benton HP, Zoumi A, Tromberg BJ, and Peavy GM, "Nonlinear optical microscopy of articular cartilage," *Osteoarthritis Cartilage* 13, 345-352 (2005),

50 Mansfield JC, Winlove CP, Moger JM, Matcher SJ, "Collagen Fibre Arrangement in Normal and Diseased Cartilage studied by Polarization Sensitive Non-Linear Microscopy", *J. Biomed. Opt.* 13(4) 044020. (2008).

51 Stoller P, Reiser KM, Celliers PM and Rubenchik AM, “Polarization-Modulated Second Harmonic Generation in Collagen”, *Biophys. J*. 82: 3330–3342 (2002).

Figures

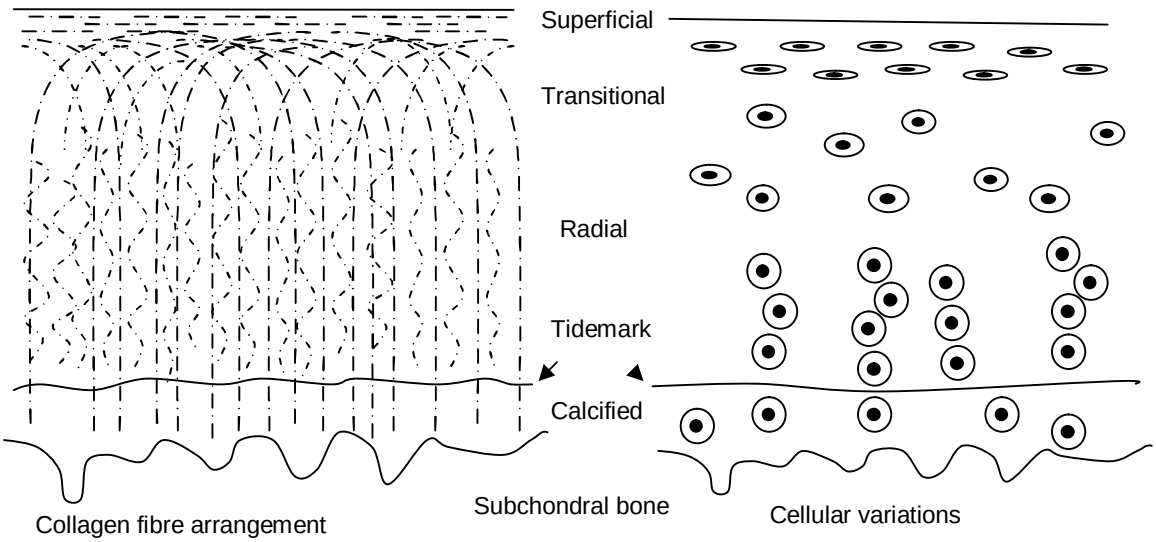

Figure 1

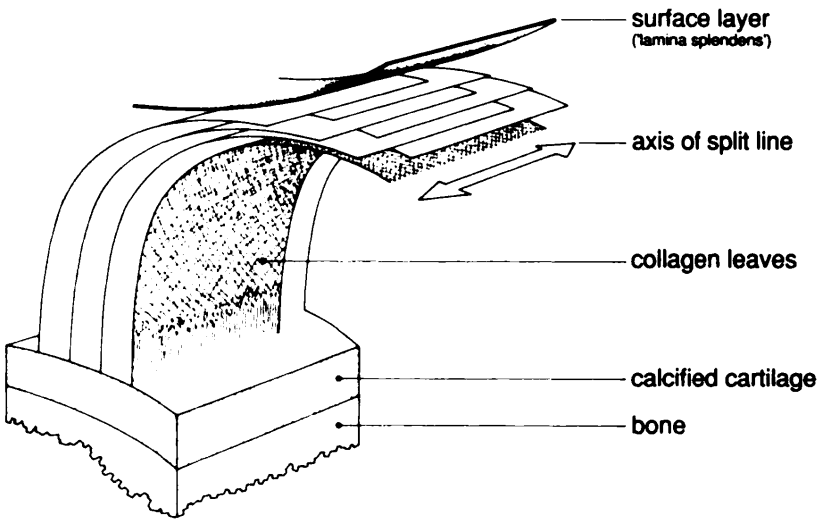
surface layer
('lamina splendens')
axis of split line
collagen leaves
calcified cartilage
bone

Figure 2.

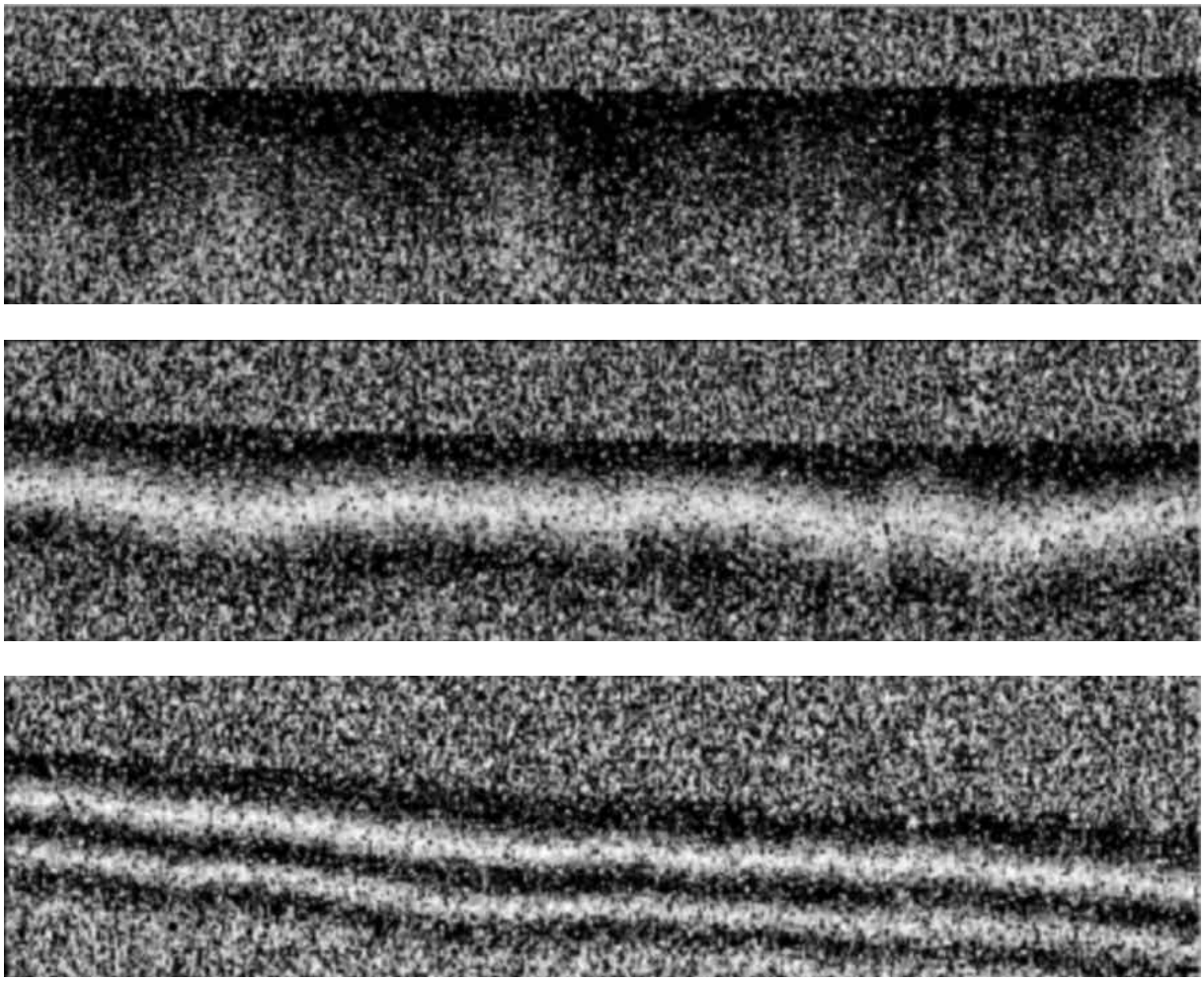

Figure 3.

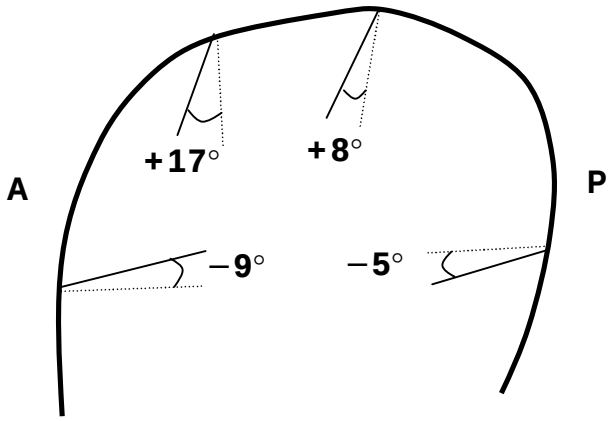

Figure 4

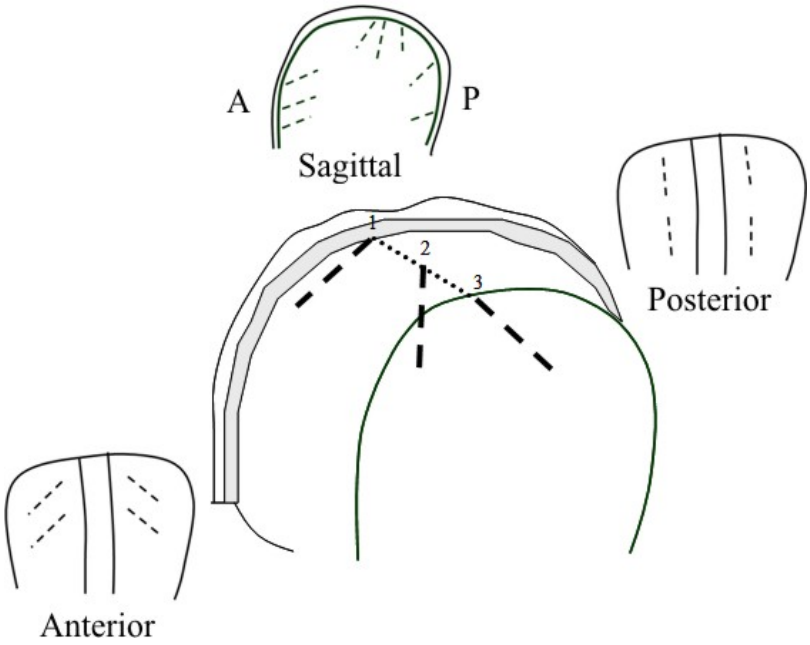

Figure 5

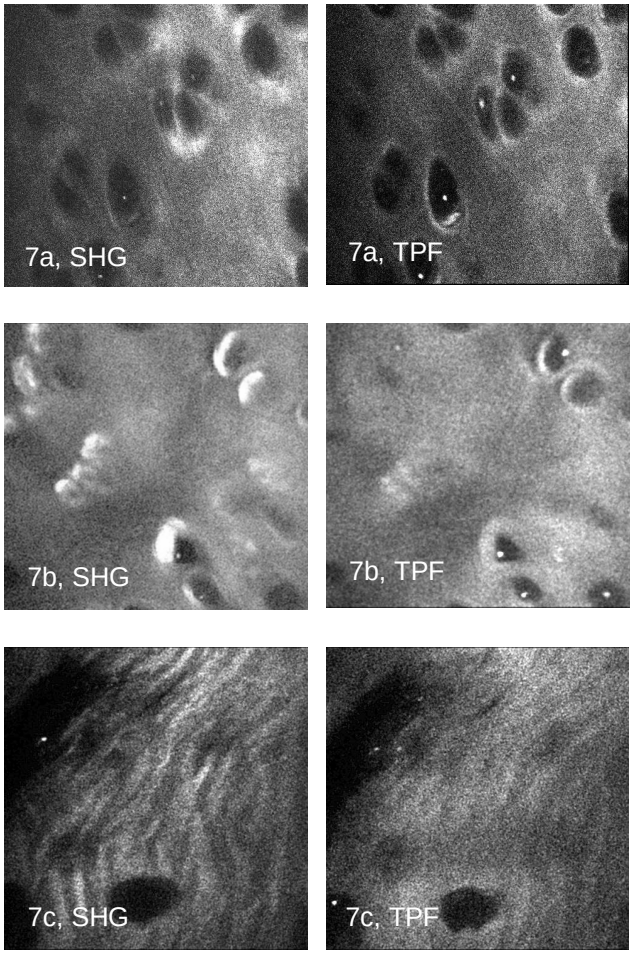

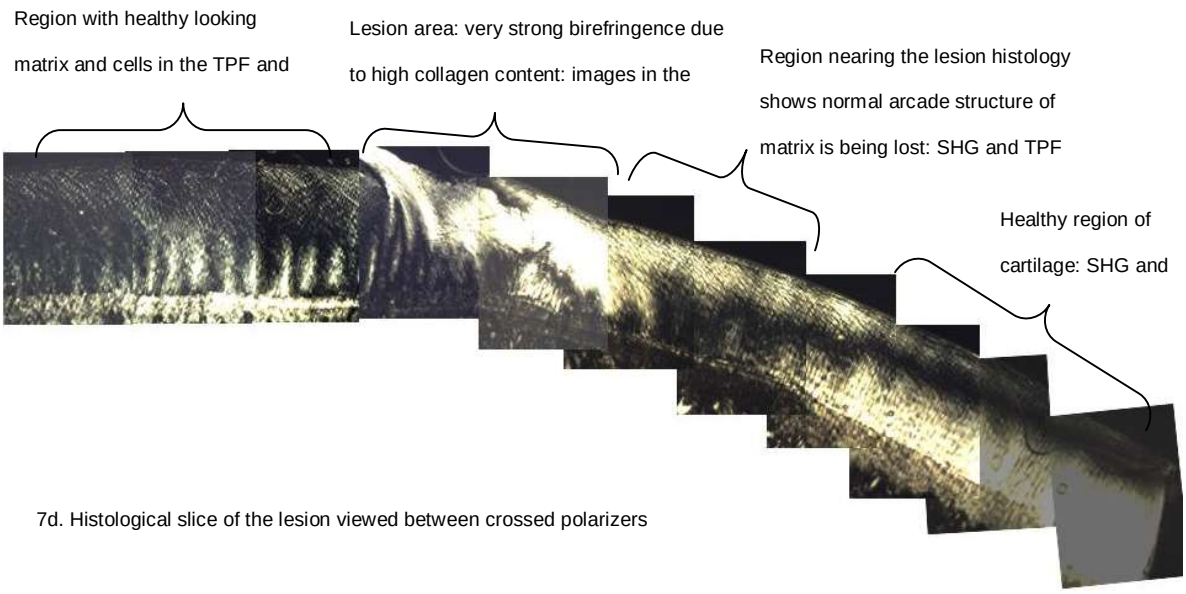

7d. Histological slice of the lesion viewed between crossed polarizers

Figure 6

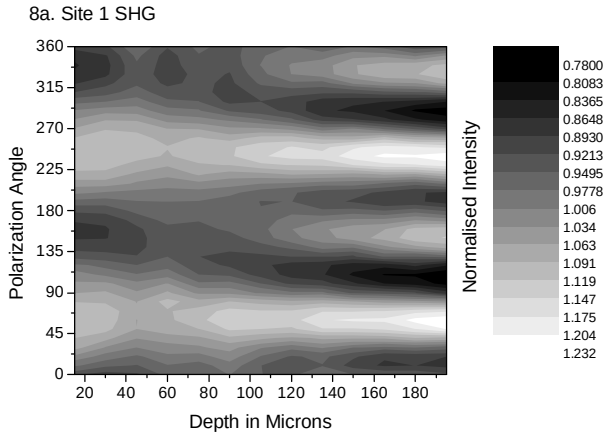
8a. Site 1 SHG
Polarization Angle
360
315
270
225
180
135
90
45
0
20 40 60 80 100 120 140 160 180
Depth in Microns
Normalised Intensity
0.7800
0.8083
0.8365
0.8648
0.8930
0.9213
0.9495
0.9778
1.006
1.034
1.063
1.091
1.119
1.147
1.175
1.204
1.232

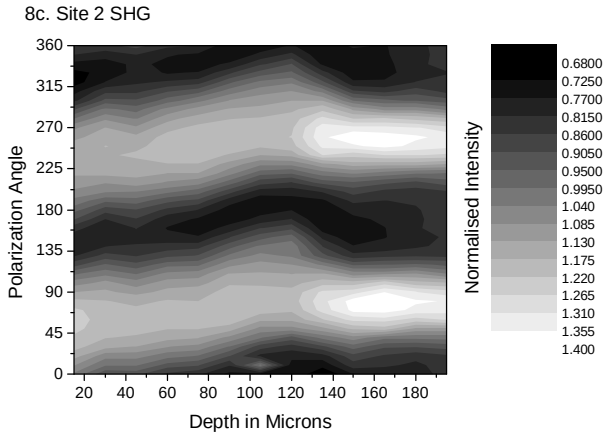
8c. Site 2 SHG
Polarization Angle
360
315
270
225
180
135
90
45
0
20 40 60 80 100 120 140 160 180
Depth in Microns
Normalised Intensity
0.6800
0.7250
0.7700
0.8150
0.8600
0.9050
0.9500
0.9950
1.040
1.085
1.130
1.175
1.220
1.265
1.310
1.355
1.400

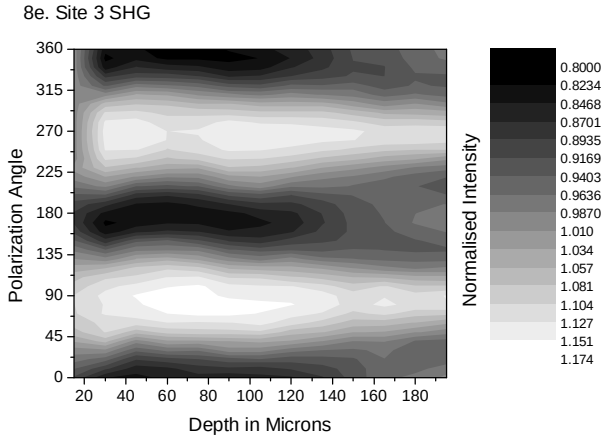
8e. Site 3 SHG
Polarization Angle
360
315
270
225
180
135
90
45
0
20 40 60 80 100 120 140 160 180
Depth in Microns
Normalised Intensity
0.8000
0.8234
0.8468
0.8701
0.8935
0.9169
0.9403
0.9636
0.9870
1.010
1.034
1.057
1.081
1.104
1.127
1.151
1.174

Figure 7

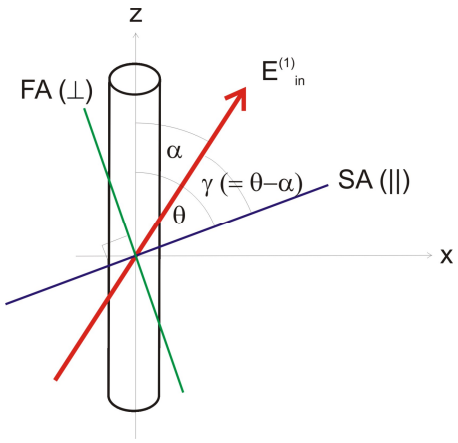

Figure 8

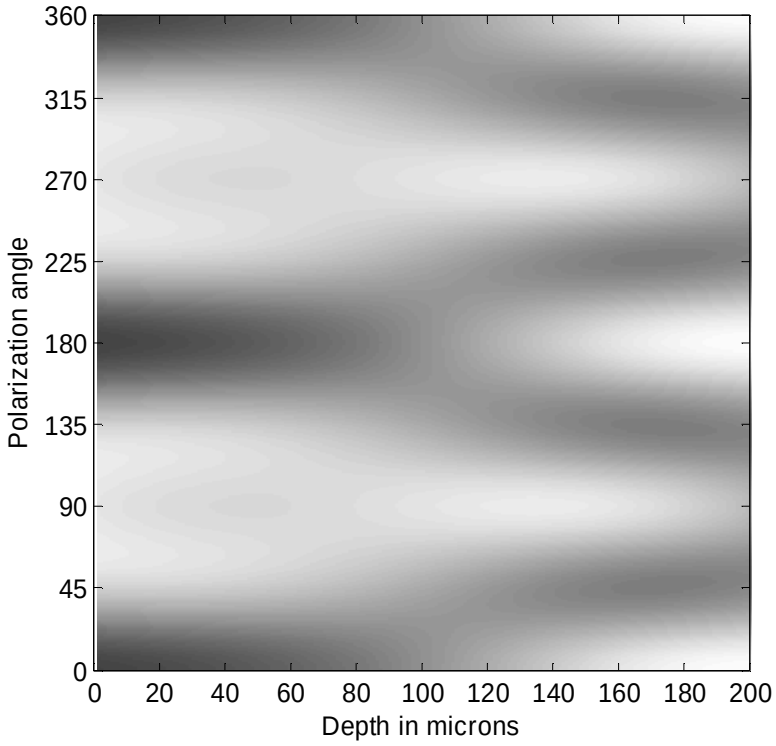
360
315
270
225
180
135
90
45
0
Polarization angle
0
20
40
60
80
100
120
140
160
180
200
Depth in microns

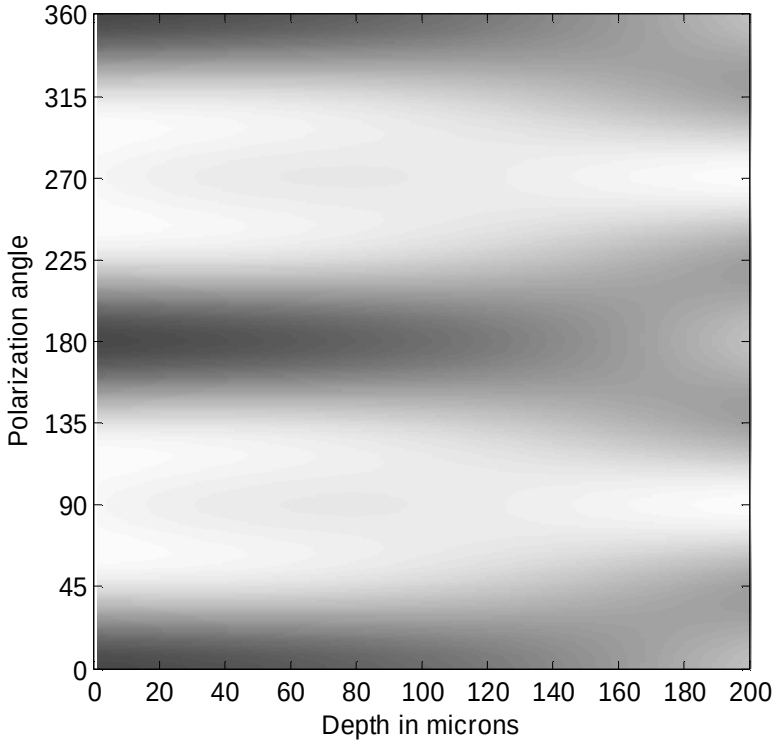
360
315
270
225
180
135
90
45
0
Polarization angle
0
20
40
60
80
100
120
140
160
180
200
Depth in microns

Figure 9